Attitude Dynamics of an Electric Sail Model with a Realistic Shape

Marco Bassetto*, Giovanni Mengali, Alessandro A. Quarta

Department of Civil and Industrial Engineering, University of Pisa, I-56122 Pisa, Italy

Abstract

The Electric Solar Wind Sail is an innovative propulsion system that gains thrust from the interaction of the incoming ions from the solar wind with an artificial electric field produced by means of long charged tethers, which are deployed and maintained stretched by rotating the spacecraft around a spin axis. Under the combined interaction between solar wind dynamic pressure and centrifugal force, the tethers reach an equilibrium configuration whose spatial shape must be known for obtaining a reasonable estimate of the propulsive acceleration, a fundamental information for preliminary mission analysis purposes. This problem has been addressed in recent papers, which deal with the analytical expressions of thrust and torque vectors of a spinning and axially-symmetric Electric Solar Wind Sail. The torque acting on the sail induces a perturbation on the orientation of the thrust vector, which is here studied by analyzing the attitude dynamics. Numerical simulations show that the spacecraft motion is characterized by an undamped precession combined with a nutation motion. The effect due to the torque acting on the spacecraft is to align the thrust direction along the Sun-sail line, thus reducing the maneuvering capabilities. This paper proposes an effective control law which is able to remove the torque by suitably adjusting the tether electric voltage. It is shown that the proposed solution maintains the nominal thrust magnitude, and requires a small electric voltage modulation.

Keywords: Electric Solar Wind Sail, thrust and torque vector model, spacecraft attitude dynamics

Nomenclature

b_l	=	dimensionless coefficient; see Eq. (35)
$\mathcal{E}$, $\mathcal{F}$, $\mathcal{G}$	=	components of $\boldsymbol{T}$ in $\mathcal{T}_B$, [N m]
f	=	distance of dx from (x_B, y_B) plane, [m]
$\boldsymbol{F}$	=	thrust vector, with $F \triangleq \|\boldsymbol{F}\|$, [N]
$\boldsymbol{F}_t$	=	projection of $\boldsymbol{F}$ on (x_B, y_B) plane, [N]
F_x, F_y, F_z	=	components of $\boldsymbol{F}$ in $\mathcal{T}_I$, [N]
h	=	dimensionless parameter; see Eq. (17)
I_t	=	transverse moment of inertia, [kg m^2]
I_z	=	longitudinal moment of inertia, [kg m^2]
$\hat{\boldsymbol{i}}$, $\hat{\boldsymbol{j}}$, $\hat{\boldsymbol{k}}$	=	unit vectors of $\mathcal{T}_B$
$\hat{\boldsymbol{i}}_I$, $\hat{\boldsymbol{j}}_I$, $\hat{\boldsymbol{k}}_I$	=	unit vectors of $\mathcal{T}_I$
k_x, k_y, k_z	=	components of $\hat{\boldsymbol{k}}$ in $\mathcal{T}_I$
L	=	tether length, [m]
$\mathcal{M}$	=	shape coefficient; see Eq. (8)
m_p	=	proton mass, [kg]

*Corresponding author

Email addresses: marco.bassetto@ing.unipi.it (Marco Bassetto), g.mengali@ing.unipi.it (Giovanni Mengali), a.quarta@ing.unipi.it (Alessandro A. Quarta)

Published in Acta Astronautica, Vol. 159 June 2019, pp. 250–257. doi: https://doi.org/10.1016/j.actaastro.2019.03.064

N	=	number of tethers
n	=	solar wind number density, $[\mathrm{m}^{-3}]$
$\mathcal{P}$	=	shape coefficient; see Eq. (8)
$\hat{\boldsymbol{r}}$	=	Sun-spacecraft unit vector
r	=	Sun-spacecraft distance, [m]
S	=	spacecraft center-of-mass
$\boldsymbol{T}$	=	torque vector, [N m]
t	=	time, [s]
u	=	solar wind speed, [m/s]
V	=	tether electric potential, [V]
V_w	=	solar wind electric potential, [V]
x	=	curvilinear abscissa, [m]
x_B, y_B, z_B	=	axes of $\mathcal{T}_B$
x_I, y_I, z_I	=	axes of $\mathcal{T}_I$
α_n	=	pitch angle, [rad]
δ_n	=	clock angle, [rad]
ϵ_0	=	vacuum permittivity, [F/m]
ζ_k	=	angular position of the k-th tether, [rad]
ϕ, θ, ψ	=	Euler's angles, [rad]
λ	=	Smelt's parameter
$\mu_\odot$	=	Sun's gravitational parameter, $[\mathrm{km}^3/\mathrm{s}^2]$
ρ	=	tether linear mass density, [kg/m]
σ	=	design parameter; see Eq. (5), [kg/m/s]
$\mathcal{T}_B$	=	body reference frame
$\mathcal{T}_I$	=	inertial reference frame
$\boldsymbol{\Omega}$	=	spacecraft angular velocity, [rad/s]
Ω_x, Ω_y, ω	=	components of $\boldsymbol{\Omega}$ in $\mathcal{T}_B$, [rad/s]

Subscripts

0	=	initial
1	=	referred to half-sail no. 1
2	=	referred to half-sail no. 2
max	=	maximum
t	=	tip

Superscripts

$'$	=	derivative with respect to x
$\cdot$	=	time derivative

1. Introduction

The Electric Solar Wind Sail (E-sail) is a propellantless propulsion system that generates a continuous thrust by exchanging momentum with solar wind particles [1, 2]. The incoming ions interact with an artificial electric field produced by means of long charged tethers, which are maintained at a voltage level on the order of a few tens of kilovolts [3]. The spacecraft spins around its symmetry axis, and this rotation is used to deploy the tethers and maintain them stretched [4, 5, 6]. The same physical principle as the E-sail concept is also used by the plasma brake device, which is a promising option for reducing the decay time of satellites in low Earth orbits at their end-of-life [7, 8, 9, 10].

In the recent literature several interplanetary mission analyses have been conducted using an E-sail as primary propulsion system [11, 12, 13]. Usually, the E-sail is described in a simplified way assuming that the tether arrangement looks like a rigid disc [14, 15]. In such an ideal configuration, the propulsive acceleration may be analytically modeled using the recent results by Huo et al. [16]. The real shape, however, is more

complex, since it results from a coupling between the solar wind dynamic pressure and the centrifugal force due to the spacecraft rotation. The problem of obtaining a more realistic description of the tether arrangement has been recently addressed in Refs. [17, 18], which deal with the analytical expressions of thrust and torque vectors of an axially-symmetric E-sail.

The results discussed in Ref. [17], which are based on the assumption of a Sun-facing sail [19, 20], show that the net thrust is aligned with the Sun-spacecraft direction, while the torque is zero. In that configuration, the equilibrium shape of each tether is well approximated by a natural logarithmic arc, provided that the E-sail spin rate is sufficiently high. This result is qualitatively in accordance with the numerical simulations by Toivanen and Janhunen [21], which show that the tethers form a cone near the spacecraft, whereas they are flattened by the centrifugal force towards the tip. Actually, the analytical approximation given in Ref. [21] estimates a parabolic shape of the tethers, with the effect of a null slope at their tip. The discrepancy between the two models is consistent with the assumption that in Ref. [21] the tips of the main tethers host remote units connected to an external rim in order to provide mechanical stability to the sail. In the presented case, instead, the remote units are not included in the model with the aim of decreasing the stress at tether root. As such, a nonzero tip slope is an expected result. The more complex case of a sail that generates a transverse thrust (and so a nonzero torque vector) is discussed by Bassetto et al. [18], whose results are obtained under the assumption that the E-sail maintains a rigid shape independent of the pitch angle α_n between the Sun-spacecraft vector $\boldsymbol{r}$ and the sail symmetry axis z_B; see Fig. 1.

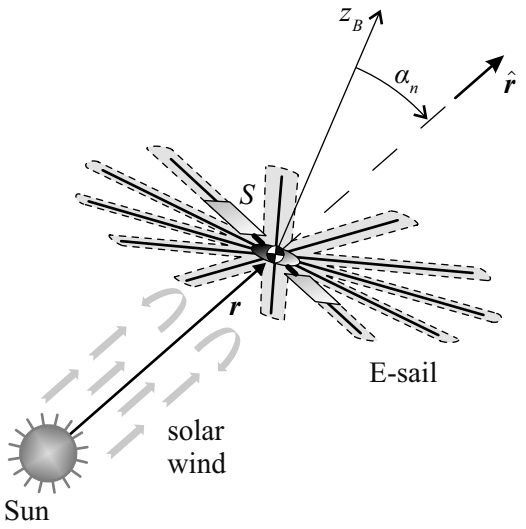

Figure 1: E-sail conceptual sketch.

Such an assumption is reasonable as long as the pitch angle is small, that is, when the tether arrangement is not far from the equilibrium shape found in a pure Sun-facing configuration. In particular, Ref. [18] introduces two dimensionless coefficients related to the E-sail shape, useful for describing the thrust and torque vectors in a compact, analytical, form. Even though these coefficients must be calculated numerically, they may be also accurately estimated with a semi-analytical approximation. As a result, closed form expressions of the E-sail propulsive characteristics are easily derived, which are very useful for both trajectory simulation, and preliminary mission analysis purposes.

The possibility of generating a trasverse thrust component is a fundamental aspect in most mission scenarios, when a change of the osculating orbit angular momentum is required. Typical examples are offered by the design of displaced [22, 23] and linear [24] trajectories, the interplanetary rendezvous [25, 26] or the outer Solar System exploration [27, 28, 29], and the rendezvous with asteroids and comets [30, 31, 32, 33, 34]. This problem has already been addressed by Toivanen et al. [35], according to which the sail attitude can be controlled by modulating the tether voltage synchronously with the sail rotation. However, the existence of a torque (induced by the bending of the tethers) acting on the spacecraft makes the analysis of its attitude dynamics an interesting problem [36]. In fact, the numerical integration of the Euler's attitude

equations shows that the spacecraft performs an undamped precession combined with nutation oscillations. In particular, the amplitude and the frequency of these two harmonic motions are affected by the initial conditions, the spacecraft inertia tensor, the number of tethers, and the electric voltage. Because the external torque makes the long-period thrust to be oriented in the radial direction, this perturbative effect must be removed.

The aim of this paper is to discuss a simple but effective control law that counteracts the generation of the external torque by suitably adjusting the tether electric voltage. Janhunen and Toivanen [37] have recently presented an algorithm to control the sail attitude. The effectiveness of such an algorithm [37] is confirmed by a full end-to-end simulation in which the tethers are modeled as elastic wires, while the solar wind characteristics are taken from historical satellite data. The same problem is here addressed in analytical way; in essence, the idea is to ideally divide the sail plane into two symmetric parts delimited by the straight line passing through the torque vector, and to assign a given value of electric voltage to each part. The value of the two control voltages is chosen such as to remove the external torque and, at the same time, to maintain the nominal thrust vector. The obtained solution shows that the required variation of electric voltage is some orders of magnitude smaller than its reference value.

The paper is organized as follows. Section 2 summarizes the torque model presented in Ref. [18], which is used in Section 3 to analyze the attitude behaviour of a rigid E-sail-based spacecraft without any voltage control. Section 4 deals with the proposed strategy to remove the external torque, while some concluding remarks are reported in the last section.

2. E-sail Model and Mathematical Preliminaries

For mathematical tractability, the spacecraft (including the E-sail) is modeled as an axially-symmetric rigid body. It is useful to introduce a principal body reference frame $\mathcal{T}_B(S; x_B, y_B, z_B)$ with unit vectors $\{\hat{\boldsymbol{i}}, \hat{\boldsymbol{j}}, \hat{\boldsymbol{k}}\}$, where $\hat{\boldsymbol{k}}$ is aligned with the spacecraft symmetry axis; see Fig. 2. The E-sail consists of an even

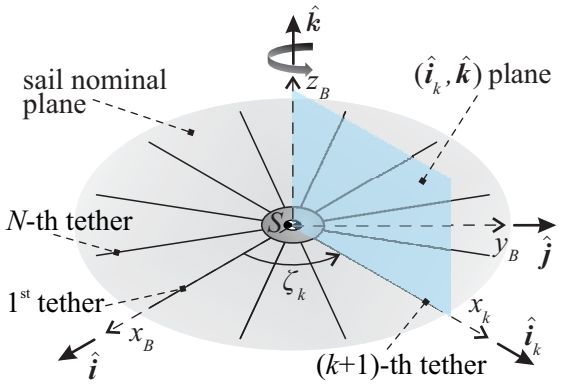

Figure 2: E-sail geometric arrangement. Adapted from Ref. [18].

number $N > 2$ of tethers, each one being denoted by a subscript k, with $k \in \{0, 1, \ldots, (N-1)\}$. The angular position of the k-th tether, measured counterclockwise on the (x_B, y_B) plane starting from x_B, is characterized by the azimuth angle

$$\zeta_k = \left(\frac{2\pi}{N}\right) k \tag{1}$$

The spacecraft attitude is described through the pitch (α_n) and clock (δ_n) angles, defined as

$$\alpha_n \triangleq \arccos(\hat{\boldsymbol{r}} \cdot \hat{\boldsymbol{k}}) \tag{2}$$

$$\delta_n \triangleq \begin{cases} \arccos\left(\dfrac{\hat{\boldsymbol{r}} \cdot \hat{\boldsymbol{i}}}{\left\|\hat{\boldsymbol{r}} \times \hat{\boldsymbol{k}}\right\|}\right) & \text{if } (\hat{\boldsymbol{r}} \cdot \hat{\boldsymbol{j}}) \geq 0 \\ 2\pi - \arccos\left(\dfrac{\hat{\boldsymbol{r}} \cdot \hat{\boldsymbol{i}}}{\left\|\hat{\boldsymbol{r}} \times \hat{\boldsymbol{k}}\right\|}\right) & \text{otherwise} \end{cases} \tag{3}$$

where $\hat{\boldsymbol{r}}$ is along the Sun-spacecraft line, which also approximately coincides with the direction of the solar wind velocity vector; see Fig. 3. In geometrical terms, $\alpha_n \in [0,\, \pi]\,\text{rad}$ is the angle between $\hat{\boldsymbol{r}}$ and the

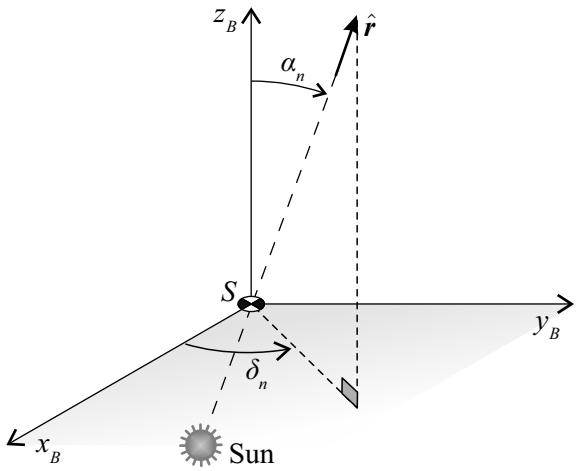

Figure 3: Pitch (α_n) and clock (δ_n) angles.

spacecraft symmetry axis (z_B), while $\delta_n \in [0,\, 2\pi]\,\text{rad}$ is the angle between x_B and the projection of $\hat{\boldsymbol{r}}$ onto the (x_B, y_B) plane. Note that δ_n is undefined when $\hat{\boldsymbol{k}}$ is parallel to $\hat{\boldsymbol{r}}$.

The mathematical model [17, 18], which is used to simulate the spacecraft attitude behavior, and then to define a control law capable of counteracting the torque acting on the E-sail when its configuration is not Sun-facing (that is, when $\hat{\boldsymbol{k}} \times \hat{\boldsymbol{r}} \neq 0$), is reassumed in the next section.

2.1. Thrust and Torque Vector Model

The thrust vector $\boldsymbol{F}$ given by an axially-symmetric E-sail may be written as [17, 18]

$$\boldsymbol{F} = \frac{1}{2}\, N\, L\, \sigma\, u\, \left[(2 - \mathcal{P})\, \hat{\boldsymbol{r}} + (3\,\mathcal{P} - 2)\, \left(\hat{\boldsymbol{r}} \cdot \hat{\boldsymbol{k}}\right)\, \hat{\boldsymbol{k}}\right] \tag{4}$$

where N is the number of tethers, L is the length of each tether, $u = 400\,\text{km/s}$ is the solar wind speed, and σ is a design parameter given by [4, 21, 38]

$$\sigma = 0.18\, \max(0,\, V - V_w)\, \sqrt{\epsilon_0\, m_p\, n} \tag{5}$$

where V is the tether voltage, V_w is the electric potential of solar wind ions (with a typical value of about 1 kV [4]), ϵ_0 is the vacuum permittivity, m_p is the proton mass, and n is the local solar wind number density. The dimensionless parameter $\mathcal{P} \in [0,\, 1]$ is related to the tether geometrical characteristics, with $\mathcal{P} = 1$ for an ideally flat sail.

The torque vector $\boldsymbol{T}$ given by an axially-symmetric E-sail can be written in compact form as [17, 18]

$$\boldsymbol{T} = \frac{1}{2}\, \mathcal{M}\, N\, L^2\, \sigma\, u\, (\hat{\boldsymbol{k}} \times \hat{\boldsymbol{r}}) \tag{6}$$

where the dimensionless coefficient $\mathcal{M} \in [0,\, 1]$ is related to the tether geometrical characteristics. In particular, the external torque vanishes ($\mathcal{M} = 0$) when the tethers are fully stretched. The magnitude of $\boldsymbol{T}$ can be expressed as

$$\|\boldsymbol{T}\| = \frac{1}{2}\,\mathcal{M}\,N\,L^2\,\sigma\,u\,\sin\alpha_n \tag{7}$$

It is worth noting that this torque induces a pitch oscillation resembling that of a spherical pendulum.

2.2. Analytical Approximation of $\mathcal{P}$ and $\mathcal{M}$

Reference [18] provides an approximation for both $\mathcal{P}$ and $\mathcal{M}$, which can be expressed as

$$\mathcal{P} \simeq 1 \quad , \quad \mathcal{M} \simeq \frac{\ln(4)\,\sigma\,u}{\rho\,\omega^2\,L} \tag{8}$$

provided that the spacecraft spin rate is sufficiently high. In Eq. (8), $\rho \simeq 10^{-5}\,\mathrm{kg/m}$ is the tether linear mass density [39], while ω is the sail spin rate. Using the approximate values of $\mathcal{P}$ and $\mathcal{M}$ given by Eq. (8), the thrust and torque vectors become

$$\boldsymbol{F} = \frac{1}{2}\,N\,L\,\sigma\,u\,\left[\hat{\boldsymbol{r}} + \left(\hat{\boldsymbol{r}}\cdot\hat{\boldsymbol{k}}\right)\,\hat{\boldsymbol{k}}\right] \tag{9}$$

$$\boldsymbol{T} = \frac{\ln(2)\,N\,L\,(\sigma\,u)^2}{\rho\,\omega^2}\,(\hat{\boldsymbol{k}}\times\hat{\boldsymbol{r}}) \tag{10}$$

In particular, the expression of the torque given by Eq. (10) is used in the next section to analyze the attitude dynamics of an E-sail-based spacecraft.

3. Spacecraft Attitude Dynamics

Under the assumption that the spacecraft behaves like a rigid body, the dimensionless coefficient $\mathcal{M}$ and the inertia tensor are both constant. The effects of the torque due to the tether inflection on the spacecraft dynamics may therefore be analyzed by numerically integrating the Euler's equations. To that end, the components of $\boldsymbol{T}$ in the body reference frame are written as a function of the three Euler's angles $\{\phi,\, \theta,\, \psi\}$, which define the orientation of $\mathcal{T}_B$ with respect to an inertial reference frame $\mathcal{T}_I(S;\, x_I,\, y_I,\, z_I)$ of unit vectors $\{\hat{\boldsymbol{\imath}}_I,\, \hat{\boldsymbol{\jmath}}_I,\, \hat{\boldsymbol{k}}_I\}$, where $\hat{\boldsymbol{k}}_I \equiv \hat{\boldsymbol{r}}$, while $\hat{\boldsymbol{\imath}}_I$ points towards a fixed direction in space. Using the rotational sequence [40] $3(\psi) \rightarrow 1(\phi) \rightarrow 2(\theta)$ to describe the orientation of $\mathcal{T}_B$ relative to $\mathcal{T}_I$, the kinematic equations of a rigid E-sail-based spacecraft are

$$\dot{\phi} = \Omega_x\,\cos\theta + \omega\,\sin\theta \tag{11}$$

$$\dot{\theta} = \Omega_y - (\omega\,\cos\theta - \Omega_x\,\sin\theta)\,\tan\phi \tag{12}$$

$$\dot{\psi} = (\omega\,\cos\theta - \Omega_x\,\sin\theta)\,\sec\phi \tag{13}$$

Let $\{\Omega_x,\, \Omega_y,\, \omega\}$ be the components of the spacecraft angular velocity in $\mathcal{T}_B$. Accordingly, the Euler's equations are

$$\dot{\Omega}_x = -h\,\omega^2\,\sin\phi + \lambda\,\Omega_y\,\omega \tag{14}$$

$$\dot{\Omega}_y = -h\,\omega^2\,\sin\theta\,\cos\phi - \lambda\,\Omega_x\,\omega \tag{15}$$

$$\dot{\omega} = 0 \tag{16}$$

with

$$h \triangleq \frac{\ln(2)\,N\,L\,(\sigma\,u)^2}{\rho\,\omega^4\,I_t} \quad , \quad \lambda \triangleq \frac{I_t - I_z}{I_t} \tag{17}$$

where I_t and I_z are the longitudinal and transverse moments of inertia, respectively. Finally, the relations between α_n and δ_n and the Euler's angles are

$$\cos\alpha_n = \cos\phi\,\cos\theta \tag{18}$$

$$\sin\alpha_n\,\sin\delta_n = \sin\phi \tag{19}$$

$$\sin\alpha_n\,\cos\delta_n = -\cos\phi\,\sin\theta \tag{20}$$

Although in principle the spacecraft attitude dynamics is affected by the rotation of $\mathcal{T}_B$ with respect to the Sun-sail line due to the vehicle orbital motion, this effect is negligible, because the spacecraft mean motion (about 1.99×10^{-7} rad/s for a circular heliocentric orbit of radius equal to 1 au) is usually several orders of magnitude smaller than the typical values of Ω_x, Ω_y and ω.

The attitude dynamics of an E-sail-based spacecraft has been analyzed for some E-sail configurations. In particular, Tab. 1 reports the characteristics of five possible E-sail arrangements, with $(N\,L) = 1000\,\mathrm{km}$, $\omega = 0.95\,\omega_{\max}$, and $V = 20\,\mathrm{kV}$. Using the configurations ① and ⑤ as exemplary cases, Eqs. (11)–(16) have

	L [km]	N	ω [rph]
E-sail ①	2	500	43.46
E-sail ②	4	250	21.73
E-sail ③	6	168	14.49
E-sail ④	8	126	10.86
E-sail ⑤	10	100	8.69

Table 1: Major specifications of five possible E-sail arrangements.

been numerically integrated with initial conditions

$$\{\alpha_{n_0},\,\delta_{n_0}\} = \{10,\,90\}\ \mathrm{deg} \tag{21}$$

$$\{\Omega_{x_0},\,\Omega_{y_0},\,\omega_0\} = \{0,\,0,\,\omega\} \tag{22}$$

assuming $\lambda = -0.5$ and $I_t = 1000\,\mathrm{kg\,m^2}$. The simulation results are illustrated in Figs. 4–7. The pitch angle shows a periodic time variation due to a nutation motion of the spacecraft symmetry axis; see Figs. 4 and 6. Both the amplitude and frequency of the nutation oscillations are higher for an E-sail with longer tethers. Moreover, introducing the components of unit vector $\hat{\boldsymbol{k}}$ in the inertial reference frame $\mathcal{T}_I$ (that is, $[\hat{\boldsymbol{k}}]_{\mathcal{T}_I} \triangleq [k_x,\,k_y,\,k_z]^{\mathrm{T}}$), Figs. 4 and 6 show that the E-sail symmetry axis is subjected to a precession motion, too. Again, the frequency of oscillation is higher for an E-sail with longer tethers.

The long-term propulsive effect due to the torque acting on the spacecraft is better visualized by representing the time evolution of the thrust vector components in the inertial reference frame, that is, $[\boldsymbol{F}]_{\mathcal{T}_I} \triangleq [F_x,\,F_y,\,F_z]^{\mathrm{T}}$. Both Figs. 5 and 7 show that the long-term thrust direction is radial, with a small-amplitude and short-period oscillations due to the nutation motion. Therefore, an active control system is necessary to counteract the effect of the external torque, thus allowing the spacecraft to give a long-term nonzero transverse thrust. This problem is discussed in the next section.

4. Torque Removal

The numerical simulations have shown that the torque acting on the spacecraft tends to re-align its spin axis with the radial direction. Such a torque must therefore be removed in order for the E-sail to generate a long-term nonzero transverse thrust. This is possible by properly adjusting the tether voltage, according to a control law that is now discussed. In the following analysis the assumption is made of small pitch angles (that is, $\alpha_n \leq 10\,\mathrm{deg}$), which implies that the tethers have approximately the same equilibrium shape as that in the Sun-facing configuration [18]. In that case, the tether shape is accurately described by a natural logarithmic arc, provided the E-sail spins at a sufficiently high rate [17]. The second approximation here introduced is that the E-sail shape does not change when the electric voltage is slightly modified from its nominal value. Actually, a realistic dynamic behaviour of each tether would require a simulation with a finite element analysis, but this issue is beyond the scope of this paper and is left to future research.

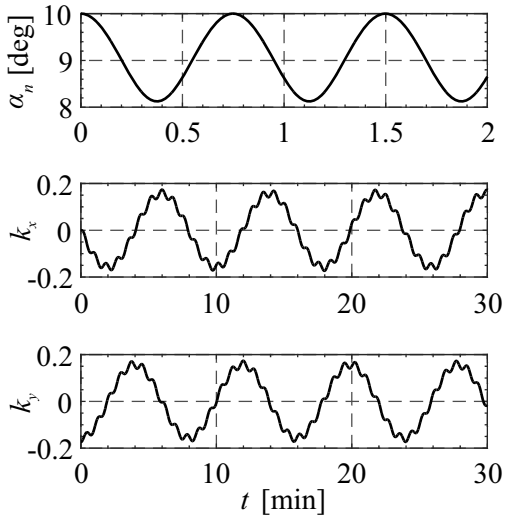

Figure 4: Time variation of α_n, k_x, and k_y for E-sail ① defined in Tab. 1.

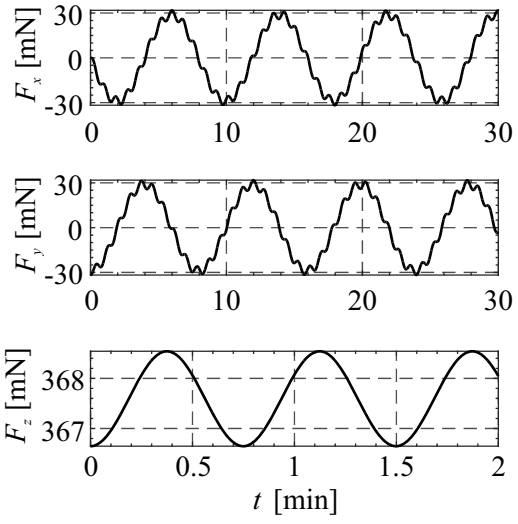

Figure 5: Time variation of $[\boldsymbol{F}]_{\mathcal{T}_I}$ for E-sail ① defined in Tab. 1.

A simple control strategy is now proposed, which consists in changing the design parameter σ with respect to its nominal value by changing the tether electric voltage; see Eq. (5). Using the results discussed in Ref. [17], the expression of $\boldsymbol{T}$ is

$$\boldsymbol{T} = \mathcal{E}\,\hat{\boldsymbol{i}} + \mathcal{F}\,\hat{\boldsymbol{j}} + \mathcal{G}\,\hat{\boldsymbol{k}} \tag{23}$$

and the problem is to look for a control law able to cancel the resultant torque. For the sake of completeness, the expressions of the components $\mathcal{E}$, $\mathcal{F}$, and $\mathcal{G}$ are reported in the Appendix. To face the problem, the tethers are first divided into two subsets by the plane passing through $\boldsymbol{T}$ and $\hat{\boldsymbol{k}}$ (referred to as partition plane), as is schematically illustrated in Fig. 8 by the dotted line. The tethers in the same subset have all the same electric potential, but those belonging to the half-plane containing the projection of the thrust on the sail nominal plane ($\boldsymbol{F}_t$) are at a higher potential (σ_2) than those belonging to the other half-plane

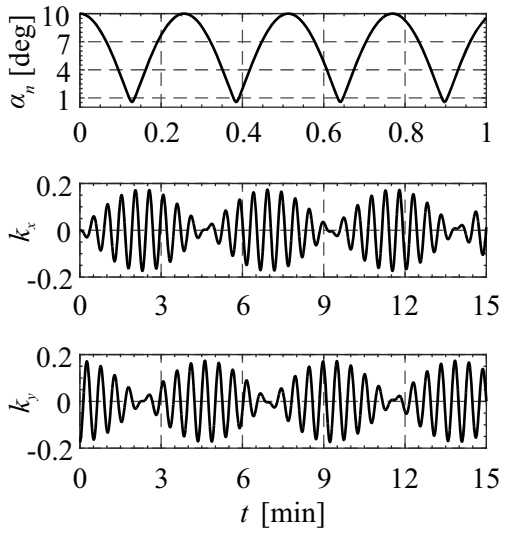

Figure 6: Time variation of α_n, k_x, and k_y for E-sail ⑤ defined in Tab. 1.

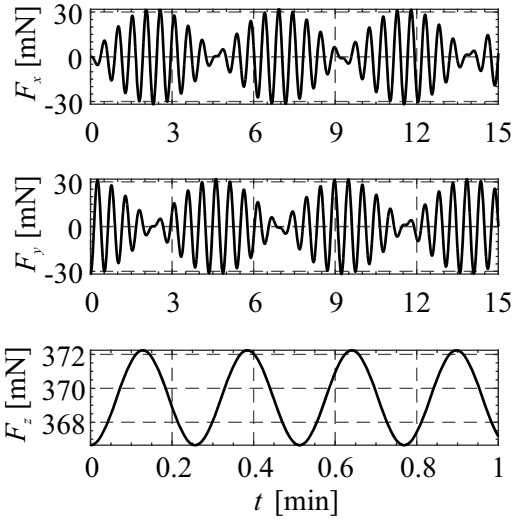

Figure 7: Time variation of $[\boldsymbol{F}]_{\mathcal{T}_I}$ for E-sail ⑤ defined in Tab. 1.

($\sigma_1 \leq \sigma_2$). Moreover, the potential of a generic tether is changed from σ_1 to σ_2 (or, viceversa, from σ_2 to σ_1) when it crosses the partition plane; see Fig. 8. With such a control strategy, the tether electric voltage must be changed every half turn of the sail about its spin axis. Note that, as long as $\sigma_2 \triangleq 2\,\sigma - \sigma_1$, the overall thrust does not vary, and therefore it is possible to maintain a fixed attitude with respect to the Sun-spacecraft line without affecting the propulsive acceleration.

With reference to the configuration of Fig. 8, the torque balance requires the following equilibrium

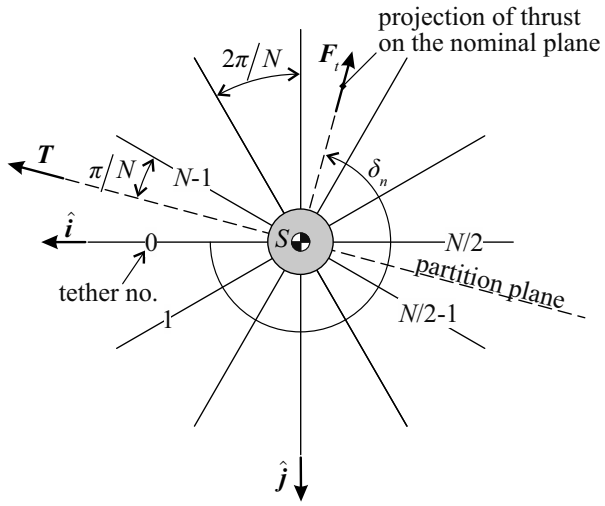

Figure 8: Sketch of a generic E-sail for attitude control determination.

conditions to be met

$$\mathcal{E} \triangleq \int_0^{x_t|_{\sigma_1}} \sum_{k=0}^{N/2-1} \mathrm{d}\mathcal{E}_k|_{\sigma_1} + \int_0^{x_t|_{\sigma_2}} \sum_{k=N/2}^{N-1} \mathrm{d}\mathcal{E}_k|_{\sigma_2} = 0 \tag{24}$$

$$\mathcal{F} \triangleq \int_0^{x_t|_{\sigma_1}} \sum_{k=0}^{N/2-1} \mathrm{d}\mathcal{F}_k|_{\sigma_1} + \int_0^{x_t|_{\sigma_2}} \sum_{k=N/2}^{N-1} \mathrm{d}\mathcal{F}_k|_{\sigma_2} = 0 \tag{25}$$

$$\mathcal{G} \triangleq \int_0^{x_t|_{\sigma_1}} \sum_{k=0}^{N/2-1} \mathrm{d}\mathcal{G}_k|_{\sigma_1} + \int_0^{x_t|_{\sigma_2}} \sum_{k=N/2}^{N-1} \mathrm{d}\mathcal{G}_k|_{\sigma_2} = 0 \tag{26}$$

where x_t is the distance of the tether tip from the spacecraft spin axis, while the whole expressions of $\mathrm{d}\mathcal{E}_k$, $\mathrm{d}\mathcal{F}_k$, and $\mathrm{d}\mathcal{G}_k$ are reported in the Appendix. With the aid of Tab. 2, the summations in Eqs. (24)–(26) give the following results

	$\sum_{k=0}^{N/2-1}$	$\sum_{k=N/2}^{N-1}$
$\sin(\zeta_k)$	$\cot(\pi/N)$	$-\cot(\pi/N)$
$\cos(\zeta_k)$	1	-1
$\sin(2\zeta_k)$	0	0
$\sin^2(\zeta_k)$	$N/4$	$N/4$
$\cos^2(\zeta_k)$	$N/4$	$N/4$

Table 2: Summations of trigonometric functions in Eqs. (24)–(26).

$$\sum_{k=0}^{N/2-1} \mathrm{d}\mathcal{E}_k|_{\sigma_1} = \Bigg[\sigma_1\, u\, \cos\alpha_n\, \cot\left(\frac{\pi}{N}\right)\, \frac{x_1 + f_1\, f_1'}{1+(f_1')^2} - \frac{N}{4}\, \sigma_1\, u\, \sin\alpha_n\, \sin\delta_n\, \frac{f_1 + x_1\, f_1' + 2\, f_1\, (f_1')^2}{1+(f_1')^2} + \\ - f_1\, \rho\, x_1\, \omega^2\, \cot\left(\frac{\pi}{N}\right)\Bigg]\, \sqrt{1+(f_1')^2}\, \mathrm{d}x_1 \tag{27}$$

$$\sum_{k=N/2}^{N-1} \mathrm{d}\mathcal{E}_k|_{\sigma_2} = \Big[-\sigma_2\, u\, \cos\alpha_n\, \cot\Big(\frac{\pi}{N}\Big)\, \frac{x_2 + f_2\, f_2'}{1+(f_2')^2} - \frac{N}{4}\, \sigma_2\, u\, \sin\alpha_n\, \sin\delta_n\, \frac{f_2 + x_2\, f_2' + 2\, f_2\, (f_2')^2}{1+(f_2')^2} +$$

$$+ f_2\, \rho\, x_2\, \omega^2\, \cot\Big(\frac{\pi}{N}\Big)\Big]\, \sqrt{1+(f_2')^2}\, \mathrm{d}x_2 \tag{28}$$

$$\sum_{k=0}^{N/2-1} \mathrm{d}\mathcal{F}_k|_{\sigma_1} = \Big[-\sigma_1\, u\, \cos\alpha_n\, \frac{x_1 + f_1\, f_1'}{1+(f_1')^2} + \frac{N}{4}\, \sigma_1\, u\, \sin\alpha_n\, \cos\delta_n\, \frac{f_1 + x_1\, f_1' + 2\, f_1\, (f_1')^2}{1+(f_1')^2} +$$

$$+ f_1\, \rho\, x_1\, \omega^2\Big]\, \sqrt{1+(f_1')^2}\, \mathrm{d}x_1 \tag{29}$$

$$\sum_{k=N/2}^{N-1} \mathrm{d}\mathcal{F}_k|_{\sigma_2} = \Big[\sigma_2\, u\, \cos\alpha_n\, \frac{x_2 + f_2\, f_2'}{1+(f_2')^2} + \frac{N}{4}\, \sigma_2\, u\, \sin\alpha_n\, \cos\delta_n\, \frac{f_2 + x_2\, f_2' + 2\, f_2\, (f_2')^2}{1+(f_2')^2} +$$

$$- f_2\, \rho\, x_2\, \omega^2\Big]\, \sqrt{1+(f_2')^2}\, \mathrm{d}x_2 \tag{30}$$

$$\sum_{k=0}^{N/2-1} \mathrm{d}\mathcal{G}_k|_{\sigma_1} = \sigma_1\, u\, x_1\, \sin\alpha_n\, \Big[\sin\delta_n - \cos\delta_n\, \cot\Big(\frac{\pi}{N}\Big)\Big]\, \sqrt{1+(f_1')^2}\, \mathrm{d}x_1 \tag{31}$$

$$\sum_{k=N/2}^{N-1} \mathrm{d}\mathcal{G}_k|_{\sigma_2} = \sigma_2\, u\, x_2\, \sin\alpha_n\, \Big[-\sin\delta_n + \cos\delta_n\, \cot\Big(\frac{\pi}{N}\Big)\Big]\, \sqrt{1+(f_2')^2}\, \mathrm{d}x_2 \tag{32}$$

where $f_i \triangleq f_i(x_i)$ describes the tether shape in the plane $(\hat{\boldsymbol{\imath}}_k,\, \hat{\boldsymbol{k}})$, while, with reference to Fig. 8, the clock angle is given by

$$\delta_n = \frac{3\pi}{2} - \frac{\pi}{N} \tag{33}$$

In order to integrate Eqs. (27)–(32), it is assumed that $f_1 \equiv f_2 = f$, that is, the shape of the E-sail corresponds to the nominal one. As stated, the latter may be approximated by a natural logarithmic arc [17], viz.

$$f \triangleq b_l\, L\, \ln\Big(1 + \frac{x}{L}\Big) \tag{34}$$

where

$$b_l \triangleq \frac{2\,\sigma\, u}{\rho\, \omega^2\, L} \tag{35}$$

Moreover, the assumptions are made that $(f')^2 \simeq 0$ and $x_t|_{\sigma_1} \equiv x_t|_{\sigma_2} \simeq L$, which are consistent with Eq. (34) and with the hypothesis of high spin rate [17, 18]. Equation (26) is satisfied for any value of σ_1, while Eqs. (24) and (25) are equivalent to each other. In particular, from Eq. (33) it may be verified that

$$\frac{\sin\delta_n}{\cot(\pi/N)} \equiv \cos\delta_n = -\sin\Big(\frac{\pi}{N}\Big) \tag{36}$$

The three integrals obtained by substituting Eq. (27) into Eq. (24) reduce to

$$\int_0^L (x + f\, f')\, \mathrm{d}x = \frac{L^2}{2}\, \Big[(b_l\, \ln 2)^2 + 1\Big] \tag{37}$$

$$\int_0^L (f + x\, f')\, \mathrm{d}x = L^2\, b_l\, \ln 2 \tag{38}$$

$$\int_0^L (x\, f)\, \mathrm{d}x = \frac{b_l\, L^3}{4} \tag{39}$$

where f is given by Eq. (34). The solution of Eq. (24) is then

$$\sigma_1 = \sigma \left\{ 1 - \frac{N \, \sin(\pi/N) \, b_l \, \ln 2}{2 \left[(b_l \, \ln 2)^2 + 1 \right]} \, \tan \alpha_n \right\} \tag{40}$$

which implies that

$$(\sigma_1 - \sigma) \propto - \tan \alpha_n \tag{41}$$

Instead, Ref. [21] shows that the voltage modulation necessary for removing the torque is proportional to a function of α_n, that is

$$(\sigma_1 - \sigma) \propto - \sin \alpha_n \, (1 + \sin \alpha_n) \tag{42}$$

Therefore, when α_n is sufficiently small, the right-hand side of both Eqs. (41) and (42) may be approximated as $-\alpha_n$. As a result, Eq. (40) is in agreement with Ref. [21] as long as $\alpha_n \ll 1$. For exemplary purposes, consider the E-sail configurations ①–⑤, whose characteristics are defined in Tab. 1. Figure 9 shows the required variation of σ_1/σ as a function α_n. Note that σ_1/σ is a monotonically decreasing function of the

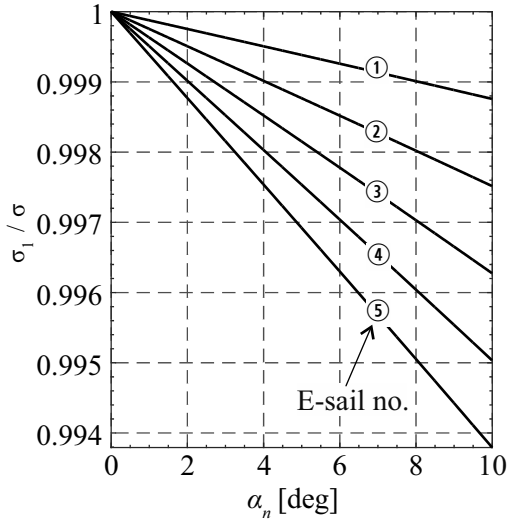

Figure 9: Variation of σ_1/σ as a function of α_n. See Tab. 1 for E-sail characteristics.

pitch angle α_n, and its value reduces as long as an E-sail with longer tethers is used. This is an expected result, since the external torque is higher when, for a given thrust magnitude, the tethers have a greater length. In particular, for a fixed value of the product $(N\,L)$, the external torque is proportional to L^2, being $\omega_{\max} \propto L^{-1}$ [18]; see Eq. (10). Note also that the required σ_1 and σ_2 are not much different from their nominal value σ; hence, the previously enforced hypothesis that $f_1 \equiv f_2 = f$ is realistic. For example, for a 5-type E-sail, and assuming $\alpha_n = 10\,\text{deg}$, we get $\sigma_1 \simeq 0.9938\,\sigma$ and $\sigma_2 \simeq 1.0062\,\sigma$. This is an interesting result, as it shows that the external torque may be counterbalanced and, correspondingly, the E-sail may be maintained at a given attitude angle with a modest modulation of the tether electric voltage.

5. Conclusions

The most recent torque model is used in this paper to analyze the attitude behaviour of an axially-symmetric E-sail-based spacecraft. In the presented model the E-sail is assumed to maintain its equilibrium shape found in a Sun-facing configuration, which is a reasonable hypothesis as long as the sail pitch angle is sufficiently small. Therefore, under the assumption of rigid body behavior, the E-sail-based spacecraft performs an undamped oscillatory motion due to the external torque, with the result that the thrust vector tends to align along the radial direction. To counteract such an effect, a simple and effective control law may be used, which consists in modulating the tether electric voltage without modifying the total thrust. The

simulations show that the tether electric voltage requires a very small variation with respect to its nominal value (on the order of 1% or less), thus allowing the E-sail to maintain a fixed attitude and, as such, to generate a long-term nonzero transverse thrust.

A natural extension of this work is represented by the formulation of a voltage control that is able to change the sail pitch angle and, at the same time, to compensate for the torque due to the tether inflection during the attitude maneuver. In particular, an interesting point to investigate is the time history of the electric voltage and the required maneuver time.

6. Appendix

With reference to Fig. 10, the torque $\mathrm{d}\boldsymbol{T}_k$ given by an infinitesimal arc-length $\mathrm{d}s_k$ of a generic tether may be expressed as [17]

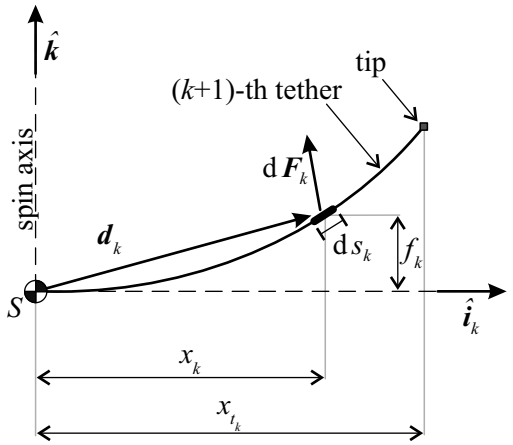

Figure 10: Geometrical representation of $\boldsymbol{d}_k$ and $\mathrm{d}\boldsymbol{F}_k$. Adapted from Ref. [17]

$$\mathrm{d}\boldsymbol{T}_k = \boldsymbol{d}_k \times \mathrm{d}\boldsymbol{F}_k \tag{43}$$

where $\boldsymbol{d}_k$ is the position vector of $\mathrm{d}s_k$ with respect to S, while $\mathrm{d}\boldsymbol{F}_k$ is the elementary force acting on $\mathrm{d}s_k$. The infinitesimal torque $\mathrm{d}\boldsymbol{T}_k$ can be rearranged by introducing the principal body frame $\mathcal{T}_B$ of unit vectors $\{\hat{\boldsymbol{i}}, \hat{\boldsymbol{j}}, \hat{\boldsymbol{k}}\}$ as

$$\mathrm{d}\boldsymbol{T}_k = \mathrm{d}\mathcal{E}_k\,\hat{\boldsymbol{i}} + \mathrm{d}\mathcal{F}_k\,\hat{\boldsymbol{j}} + \mathrm{d}\mathcal{G}_k\,\hat{\boldsymbol{k}} \tag{44}$$

where

$$\begin{aligned}\mathrm{d}\mathcal{E}_k = \Bigg\{ & x_k\,\sin\zeta_k \left[\sigma_k\,u\,\cos\alpha_n - \frac{f_k'\,\sigma_k\,u\,(\sin\alpha_n\,\cos(\delta_n-\zeta_k) + f_k'\,\cos\alpha_n)}{1+(f_k')^2}\right] + \\ & -f_k\,\sin\zeta_k \left[\rho\,x_k\,\omega^2 - \frac{\sigma_k\,u\,(\sin\alpha_n\,\cos(\delta_n-\zeta_k) + f_k'\,\cos\alpha_n)}{1+(f_k')^2}\right] + \\ & -f_k\,\sigma_k\,u\,\sin\alpha_n\,\sin\delta_n\Bigg\}\,\sqrt{1+(f_k')^2}\,\mathrm{d}x_k\end{aligned} \tag{45}$$

$$\mathrm{d}\mathcal{F}_k = \Bigg\{ -x_k\,\cos\zeta_k \left[\sigma_k\,u\,\cos\alpha_n - \frac{f'_k\,\sigma_k\,u\,(\sin\alpha_n\,\cos(\delta_n-\zeta_k)+f'_k\,\cos\alpha_n)}{1+(f'_k)^2} \right] +$$

$$+ f_k\,\cos\zeta_k \left[\rho\,x_k\,\omega^2 - \frac{\sigma_k\,u\,(\sin\alpha_n\,\cos(\delta_n-\zeta_k)+f'_k\,\cos\alpha_n)}{1+(f'_k)^2} \right] +$$

$$+ f_k\,\sigma_k\,u\,\sin\alpha_n\,\cos\delta_n \Bigg\}\,\sqrt{1+(f'_k)^2}\,\mathrm{d}x_k \quad (46)$$

$$\mathrm{d}\mathcal{G}_k = \sigma_k\,u\,x_k\,\sin\alpha_n\,\sin(\delta_n-\zeta_k)\,\sqrt{1+(f'_k)^2}\,\mathrm{d}x_k \quad (47)$$

The torque $\boldsymbol{T}_k$ acting on the k-th tether is therefore provided by

$$\boldsymbol{T}_k = \int_0^{x_{t_k}} \mathrm{d}\boldsymbol{T}_k = \mathcal{E}_k\,\hat{\boldsymbol{i}} + \mathcal{F}_k\,\hat{\boldsymbol{j}} + \mathcal{G}_k\,\hat{\boldsymbol{k}} \quad (48)$$

where

$$\mathcal{E}_k \triangleq \int_0^{x_{t_k}} \mathrm{d}\mathcal{E}_k \quad , \quad \mathcal{F}_k \triangleq \int_0^{x_{t_k}} \mathrm{d}\mathcal{F}_k \quad , \quad \mathcal{G}_k \triangleq \int_0^{x_{t_k}} \mathrm{d}\mathcal{G}_k \quad (49)$$

whereas the total torque $\boldsymbol{T}$ acting on the E-sail is

$$\boldsymbol{T} = \sum_{k=0}^{N-1} \boldsymbol{T}_k \equiv \mathcal{E}\,\hat{\boldsymbol{i}} + \mathcal{F}\,\hat{\boldsymbol{j}} + \mathcal{G}\,\hat{\boldsymbol{k}} \quad (50)$$

in which

$$\mathcal{E} \triangleq \sum_{k=0}^{N-1} \mathcal{E}_k \quad , \quad \mathcal{F} \triangleq \sum_{k=0}^{N-1} \mathcal{F}_k \quad , \quad \mathcal{G} \triangleq \sum_{k=0}^{N-1} \mathcal{G}_k \quad (51)$$

References

[1] P. Janhunen, Electric sail for spacecraft propulsion, Journal of Propulsion and Power 20 (4) (2004) 763–764, doi: 10.2514/1.8580.

[2] P. Janhunen, Status report of the electric sail in 2009, Acta Astronautica 68 (5-6) (2011) 567–570, doi: 10.1016/j.actaastro.2010.02.007.

[3] P. Janhunen, A. Sandroos, Simulation study of solar wind push on a charged wire: basis of solar wind electric sail propulsion, Annales Geophysicae 25 (3) (2007) 755–767, doi: 10.5194/angeo-25-755-2007.

[4] P. Janhunen, P. K. Toivanen, J. Polkko, et al., Electric solar wind sail: Toward test missions, Review of Scientific Instruments 81 (11) (2010) 111301–1–11301–11, doi: 10.1063/1.3514548.

[5] P. Janhunen, A. A. Quarta, G. Mengali, Electric solar wind sail mass budget model, Geoscientific Instrumentation, Methods and Data Systems 2 (1) (2013) 85–95, doi: 10.5194/gi-2-85-2013.

[6] J. Fulton, H. Schaub, Fixed-axis electric sail deployment dynamics analysis using hub-mounted momentum control, Acta Astronautica 144 (2018) 160–170, doi: 10.1016/j.actaastro.2017.11.048.

[7] P. Janhunen, Electrostatic plasma brake for deorbiting a satellite, Journal of Propulsion and Power 26 (2) (2010) 370–372, doi: 10.2514/1.47537.

[8] L. Orsini, L. Niccolai, G. Mengali, A. A. Quarta, Plasma brake model for preliminary mission analysis, Acta Astronautica 144 (2018) 297–304, doi: 10.1016/j.actaastro.2017.12.048.

[9] L. Niccolai, M. Bassetto, A. A. Quarta, G. Mengali, Plasma brake approximate trajectory. Part I: Geocentric motion, Advances in the Astronautical Sciences 163 (2018) 235–248 .

[10] M. Bassetto, L. Niccolai, A. A. Quarta, G. Mengali, Plasma brake approximate trajectory. Part II: Relative motion, Advances in the Astronautical Sciences 163 (2018) 249–259 .

[11] G. Mengali, A. A. Quarta, P. Janhunen, Electric sail performance analysis, Journal of Spacecraft and Rockets 45 (1) (2008) 122–129, doi: 10.2514/1.31769.

[12] P. Janhunen, The electric sail - a new propulsion method which may enable fast missions to the outer Solar System, Journal of the British Interplanetary Society 61 (8) (2008) 322–325 .

[13] P. Janhunen, The electric solar wind sail status report, in: European Planetary Science Congress 2010, Vol. 5, European Planetology Network and the European Geosciences Union, 2010, paper EPSC 2010-297.

[14] K. Yamaguchi, H. Yamakawa, Study on orbital maneuvers for electric sail with on-off thrust control, Aerospace Technology Japan, the Japan Society for Aeronautical and Space Sciences 12 (2013) 79–88, doi: 10.2322/astj.12.79.

[15] A. A. Quarta, G. Mengali, Minimum-time trajectories of electric sail with advanced thrust model, Aerospace Science and Technology 55 (2016) 419–430, doi: 10.1016/j.ast.2016.06.020.

[16] M. Huo, G. Mengali, A. A. Quarta, Electric sail thrust model from a geometrical perspective, Journal of Guidance, Control and Dynamics 41 (3) (2018) 735–741, doi: 10.2514/1.G003169.
[17] M. Bassetto, G. Mengali, A. A. Quarta, Thrust and torque vector characteristics of axially-symmetric E-sail, Acta Astronautica 146 (2018) 134–143, doi: 10.1016/j.actaastro.2018.02.035.
[18] M. Bassetto, G. Mengali, A. A. Quarta, Stability and control of spinning E-sail in heliostationary orbit, Journal of Guidance, Control, and Dynamics 42 (2019) 425–431, doi: 10.2514/1.G003788.
[19] G. Mengali, A. A. Quarta, G. Aliasi, A graphical approach to electric sail mission design with radial thrust, Acta Astronautica 82 (2) (2013) 197–208, doi: 10.1016/j.actaastro.2012.03.022.
[20] A. A. Quarta, G. Mengali, Analysis of electric sail heliocentric motion under radial thrust, Journal of Guidance, Control and Dynamics 39 (6) (2016) 1431–1435, doi: 10.2514/1.G001632.
[21] P. K. Toivanen, P. Janhunen, Thrust vectoring of an electric solar wind sail with a realistic sail shape, Acta Astronautica 131 (2017) 145–151, doi: 10.1016/j.actaastro.2016.11.027.
[22] L. Niccolai, A. A. Quarta, G. Mengali, Electric sail-based displaced orbits with refined thrust model, Proceedings of the Institution of Mechanical Engineers, Part G: Journal of Aerospace Engineering 232 (3) (2018) 423–432, doi: 10.1177/0954410016679195.
[23] L. Niccolai, A. A. Quarta, G. Mengali, Electric sail elliptic displaced orbits with advanced thrust model, Acta Astronautica 138 (2017) 503–511, doi: 10.1016/j.actaastro.2016.10.036.
[24] A. A. Quarta, G. Mengali, Optimal solar sail transfer to linear trajectories, Acta Astronautica 82 (2) (2013) 189–196, doi: 10.1016/j.actaastro.2012.03.005.
[25] P. Janhunen, S. Merikallio, M. Paton, EMMI - electric solar wind sail facilitated manned Mars initiative, Acta Astronautica 113 (2015) 22–28, doi: 10.1016/j.actaastro.2015.03.029.
[26] P. Janhunen, P. K. Toivanen, Safety criteria for flying E-sail through solar eclipse, Acta Astronautica 114 (2015) 1–5, doi: 10.1016/j.actaastro.2015.04.006.
[27] G. Mengali, A. A. Quarta, P. Janhunen, Considerations of electric sailcraft trajectory design, Journal of the British Interplanetary Society 61 (8) (2008) 326–329 .
[28] A. A. Quarta, G. Mengali, Electric sail mission analysis for outer Solar System exploration, Journal of Guidance, Control, and Dynamics 33 (3) (2010) 740–755, doi: 10.2514/1.47006.
[29] P. Janhunen, J.-P. Lebreton, S. Merikallio, M. Paton, G. Mengali, A. A. Quarta, Fast E-sail Uranus entry probe mission, Planetary and Space Science 104 (2014) 141–146, doi: 10.1016/j.pss.2014.08.004.
[30] A. A. Quarta, G. Mengali, Electric sail missions to potentially hazardous asteroids, Acta Astronautica 66 (9-10) (2010) 1506–1519, doi: 10.1016/j.actaastro.2009.11.021.
[31] A. A. Quarta, G. Mengali, P. Janhunen, Electric sail for a near-Earth asteroid sample return mission: Case 1998 KY26, Journal of Aerospace Engineering 27 (6) (2014) , doi: 10.1061/(ASCE)AS.1943-5525.0000285.
[32] G. Mengali, A. A. Quarta, Optimal nodal flyby with near-Earth asteroid using electric sail, Acta Astronautica 104 (2) (2014) 450–457, doi: 10.1016/j.actaastro.2014.02.012.
[33] A. A. Quarta, G. Mengali, P. Janhunen, Electric sail option for cometary rendezvous, Acta Astronautica 127 (2016) 684–692, doi: 10.1016/j.actaastro.2016.06.020.
[34] M. Bassetto, A. A. Quarta, G. Mengali, Locally-optimal electric sail transfer, Proceedings of the Institution of Mechanical Engineers, Part G: Journal of Aerospace Engineering, 233 (1) (2019) 166–179, doi: 10.1177/0954410017728975.
[35] P. K. Toivanen, P. Janhunen, J. Envall, Electric sail control mode for amplified transverse thrust, Acta Astronautica 106 (2015) 111–119, doi: 10.1016/j.actaastro.2014.10.031.
[36] C. Montalvo, B. Wiegmann, Electric sail space flight dynamics and controls, Acta Astronautica 148 (2018) 268–275, doi: 10.1016/j.actaastro.2018.05.009.
[37] P. Janhunen, P. K. Toivanen, A scheme for controlling the E-sail's spin rate by the E-sail effect itself, in: Space Propulsion 2018, Seville, Spain, 2018.
[38] P. K. Toivanen, P. Janhunen, Spin plane control and thrust vectoring of electric solar wind sail, Journal of Propulsion and Power 29 (1) (2013) 178–185, doi: 10.2514/1.B34330.
[39] H. Seppänen, T. Rauhala, S. Kiprich, J. Ukkonen, M. Simonsson, R. Kurppa, P. Janhunen, E. Hæggström, One kilometer (1 km) electric solar wind sail tether produced automatically, Review of Scientific Instruments 84 (9) (2013) , doi: 10.1063/1.4819795.
[40] J. R. Wertz (Ed.), Spacecraft Attitude Determination and Control, 1st Edition, Astrophysics and Space Science Library, Springer Netherlands, Dordrecht, Holland, 1978, pp. 760–766.